Int. J. Electron. Commun. (AEÜ) 143 (2022) 154040

Contents lists available at ScienceDirect

International Journal of Electronics and Communications

journal homepage: www.elsevier.com/locate/aeue

A novel low-pass filter based on dielectric impedance inverters to enhance the multipactor breakdown threshold

Antonio Romera Perez [a], Alejandro Pons Abenza [b], Fernando D. Quesada Pereira [a,*], Juan Hinojosa Jimenez [a], Alejandro Alvarez Melcon [a], Juan Sebastian Gomez Diaz [c]

[a] Communications and Information Technologies Department, Universidad Politécnica de Cartagena, Campus de la Muralla del Mar s/n, Cuartel de Antigones, Cartagena 30202, Spain
[b] Department of Computer Science, Universidad de Alcalá (UAH), Escuela Politécnica, Campus Universitario, Ctra.Madrid-Barcelona, km. 33, 600 28805, Alcalá de Henares, Madrid, Spain
[c] Department of Electrical and Computer Engineering, University of California at Davis, Davis, CA 95616, USA

ARTICLE INFO

Keywords:
Waveguide low-pass filter
Microwave filters
Multipactor breakdown
Dielectric filter

ABSTRACT

This work presents a novel low-pass filter based on using dielectric materials, in the critical areas of the structure, to prevent high-power space condition adverse effects, like multipactor breakdown. It is shown that the use of dielectric pieces in the inverters of the filter leads to increased gaps between metallic parts in the irises. In addition, by completely filling up the air space in critical gaps, the multipactor breakdown thresholds can be increased. Moreover, they also lead to a volume reduction, increasing compactness of the structure. To demonstrate the proposed concept, a prototype has been manufactured with an aluminum housing and a Teflon dielectric material, and tested for multipactor effect at ESA-VSC Laboratory. Tests confirmed that the manufactured filter has good electrical performance with cut-off frequency 13.6 GHz, insertion losses 0.32 dB, return losses better than 15 dB, and additionally does not show multipactor breakdown up to the maximum power tested in the experimental facility (5.5 kW).

1. Introduction

Waveguide filters are ubiquitous components in RF technology Cameron et al. [1]. In certain scenarios, including space communications, particle accelerators, and microwave tubes such as cyclotrons, waveguide filters should be able to handle high-power phenomena, such as multipactor effect Vaughan [2], Gallagher [3], San-Blas et al. [4] and corona discharge Pinheiro-Ortega et al. [5], Gharehkand [6], to avoid unwanted damage. In particular, the multipactor effect is a self-sustained electron avalanche that occasionally appears in waveguides or certain components between metallic surfaces. This phenomenon is triggered when a free electron impinges with enough energy on a metallic plate and releases out additional electrons due to the secondary emission yield (SEY) effect Walker et al. [7], leading to an exponential electron multiplication growth, that can cause unwanted electrical responses or even the destruction of the device.

Unfortunately, common waveguide filters are prone to multipactor breakdown Cameron et al. [1]. For instance, low-pass filters based on capacitive irises possess small gaps that significantly reduces their multipactor breakdown power thresholds Wolk et al. [8], Al-Mudhafar et al. [9]. This response appears due to the increased concentration of electrons in a given area after they have impacted on the metallic surface of the iris, and can be predicted from multipactor susceptibility charts Udiljak et al. [10]. Multipactor breakdown also appears in ridge waveguide bandpass filters Gonzalez-Iglesias et al. [11]. In such configurations, small gaps between adjacent ridges are usually included to increase the spurious free-range of the filters. However, the interplay between small geometrical features and sharp corners leads to a local enhancement of the induced electric fields that reduces the filter power-handling capabilities. Similar trade-off between spurious free-range and power handling also occurs in low-pass filters based on stepped impedances Cameron et al. [1].

One possible strategy to mitigate this challengue is to avoid using sharp corners and instead employ alternative geometries that increase the scattering of free electrons out of the critical regions. For instance, capacitive rounded posts have been proposed to implement rectangular

* Corresponding author.
E-mail addresses: antoniorp89@gmail.com (A. Romera Perez), alejandroponsabenza@gmail.com (A. Pons Abenza), fernando.quesada@upct.es (F.D. Quesada Pereira), juan.hinojosa@upct.es (J. Hinojosa Jimenez), alejandro.alvarez@upct.es (A. Alvarez Melcon), jsgomez@ucdavis.edu (J.S. Gomez Diaz).

https://doi.org/10.1016/j.aeue.2021.154040
Received 22 June 2021; Accepted 12 November 2021
Available online 16 November 2021

waveguide low-pass filters Vera-Castejon et al. [12]. These rounded posts deviate the electrons scattered after their impact on critical gaps, increasing the power-handling capabilities of the filter. Another alternative consists in employing a wedge-shaped waveguide along the propagation axis to implement a bandpass filter Gonzalez et al. [13], Hueso et al. [14,15]. The slanted shape of the waveguide eases the scattering of free electrons out of critical areas, improving the multipactor breakdown power threshold. Following the aforementioned ideas, "wavy" shaped designs have also been proposed and demonstrated Arregui et al. [16], Arregui et al. [17,18]. This latter design significantly reduces the multipactor risk by more than one order of magnitude as compared to a baseline corrugated lowpass filter. Nevertheless, non standard additive manufacturing techniques, such as electroforming, are needed to fabricate the complex shapes of this kind of wavy filters. In addtion, although the curved gaps lead to lesser electron multipactor avalanch effects, these are not completely avoided, since their free movement in critical areas is still possible.

A different approach consists in using various materials, such as ferrites Gonzalez-Iglesias et al. [19] or dielectrics Coves et al. [20], to enhance the multipactor breakdown power threshold. For instance, ferrite materials are known to improve the multipactor breakdown threshold at high frequencies Gonzalez-Iglesias et al. [21]. In addition, dielectric materials can also increase the multipactor breakdown power threshold. For instance, Penalva et al. [22] demostrates that a dielectric slab placed on the bottom wall of a parallel plate waveguide leads to a much better multipactor susceptibility chart as compared to the one obtained for an empty parallel plate waveguide.

Moreover, Hu and Cui [23] proposed an E-plane impedance transformer whose inner parts are filled with a dielectric material. This device does not exhibit any multipactor discharge in experimental tests up to certain power level limited by the employed testbed. Thus, the use of dielectric materials in structures, where it is likely to occur a multipactor phenomenon, seems to be a valid approach to increase the multipactor breakdown power threshold in RF devices. However, this last approach has not yet been applied to more complex microwave devices like microwave filters, that require specially tailored design techniques to account for these additional dielectric parts.

In the case of space communication applications, especially suited dielectric materials can be used to enhance the multipactor breakdown threshold as shown in Vague et al. [24]. In this latter work, the multipactor power handling capabilities of a lowpass coaxial waveguide filter were studied, after introducing different kinds of dielectric materials coating its innermost and most critical section. There is one important difference between these two last works. In Hu and Cui [23] the main goal was the mitigation of the multipactor breakdown effect by introducing a dielectric piece that completely fills the criticall gaps. On the contrary, the motivation of Vague et al. [24] was the assesment of the multipactor power thresholds when the metallic walls of the gaps were coated by different dielectric materials. As it was demostrated in this study, only small improvements in multipactor power thresholds were obtained by keeping the air gaps and simply coating the metallic parts with dielectrics. Therefore, we can conclude that improvements in multipactor risk when employing dielectric materials are mainly achieved when they completely fill the whole volume of the critical gaps, consequently avoiding the movement of free electrons in these regions.

In this context, we present the analysis, design, and experimental demonstration of a new type of rectangular waveguide low-pass filters based on capacitive irises with high multipactor threshold and wide spurious free-range. The idea is based on placing dielectric material pieces filling those critical areas where the multipactor breakdown phenomenon would more likely be triggered. In this way, the free electron movement in these tight gaps is completely avoided. This configuration leads to a significant improvement in the multipactor breakdown power threshold, in relation to classical fully metallic filter implementations, as recognized for an impedance transformer in Hu and Cui [23]. A traditional all metallic capacitive low-pass rectangular waveguide filter with similar specifications has been designed as a reference. This device is limited by a 4 kW multipactor breakdown power threshold computed with an accurate software tool (using CST-FEST3D 2021 Dassault-Systemes [25] high-power module), while we have experimentally tested our prototype at the European High-Power RF Space Laboratory ESA-VSC [26]. The new filter does not show any multipactor breakdown up to 5.5 kW, which is the maximum power that could be employed in this test facility.

This work is organized as follows. Section 2 introduces a novel type of impedance inverter filled with a dielectric material, which is the building block of the proposed filters. At that point, we discuss the advantages and drawbacks of employing dielectric-filled pieces in inverters and describe a systematic design procedure to synthesize low-pass filters. Section 3 presents a low-pass filter implemented by using these new kind of impedance inverters. Finally, Section 4 gives details about the fabricated prototype and its experimental characterization, including the frequency response and power handling aspects, demonstrating high multipactor breakdown. The filter is then compared with respect to the baseline filter with similar electrical characteristics, but implemented with all metallic parts. The multipactor power threshold estimated for the all metalic baseline filter is significantly lower. This test experimentally demonstrates the improvement in multipactor power thresholds that can be achieved with the new proposed structure.

2. Filter design procedure and impedance inverter characterization

In order to synthesize a low-pass filter, the design technique presented in Vera-Castejon et al. [12], Mximo-Gutirrez et al. [27], based on a stepped impedance implementation, is adopted. Following this technique, the low-pass filter is represented with an equivalent circuit based on impedance inverters and transmission line sections, as shown in Fig. 1. The design technique takes as specifications the order of the filter N, the return loss level RL and the electrical length of the transmission lines that connect the impedance inverters θ_c (see Fig. 1). This electrical length (θ_c) determines the spurious free-range of the filter. The characteristic impedance of the inner transmissions lines (Z_0) is the same as those used in the input and output waveguide sections.

This low-pass filter equivalent circuit can be segmented in several subcircuits composed of individual impedance inverters connected to two transmission lines of electrical length $\theta_c/2$, as shown in Fig. 2. In order to enhance the multipactor breakdown power threshold, this ideal impedance inverter is implemented, in this work, utilizing the geometry shown in Fig. 3. As can be observed, it comprises a regular capacitive step inside a rectangular waveguide, but completely covered with a dielectric piece. Therefore, there are no vacuum gaps in critical areas where free electrons can move. We should stress that this configuration does not avoid the possible side multipactor effect in areas outside the iris. However, due to weak fields and large gaps far from the irises, multipactor risk is expected to be very low in these areas. The dielectric piece parameters d_x,d_y, and d_z and also the iris thickness t_i are selected in advanced to ensure that the mechanical piece is practically feasible (see Fig. 3). We have carried out a parametric study on the electrical effect introduced by these parameters (d_x, d_y and d_z) on the inverter response. We have observed that slightly changing d_x leads to very small variations in the inverter behavior, since this modifies a region close to the side rectangular waveguide walls where the field level is negligible. On the other hand, a stronger effect is produced when d_y and specially d_z are altered. In this case, the size of the dielectric along the propagation direction, in a rectangular waveguide region with important field level, is modified. Therefore, this is translated into a variation in magnitude and phase in the inverter response. However, this effect is incorporated during the design procedure and does not suppose any difficulty, since these parameters are fixed from the starting point of the design process.

The value of the normalized inverter K/Z_0 can be obtained through

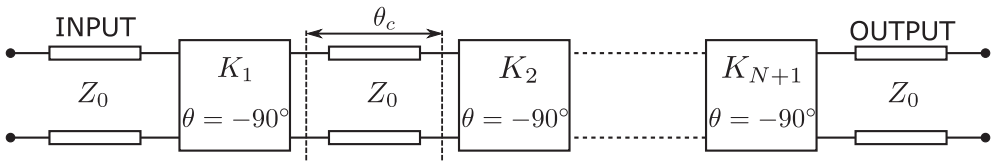

Fig. 1. Low-pass filter equivalent circuit, using impedance inverters, obtained from the stepped impedance synthesis technique proposed in Vera-Castejon et al. [12]. The filter is composed of $N+1$ capacitive impedance inverters ($\theta = -90°$) connected through N transmission lines of electrical length θ_c and characteristic impedance Z_0.

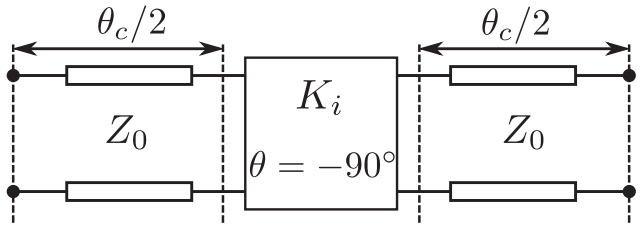

Fig. 2. One of the segments of the equivalent circuit shown in Fig. 1. It is made up of an impedance inverter (K_i) and two transmission line sections of characteristic impedance Z_0 and electrical length $\theta_c/2$.

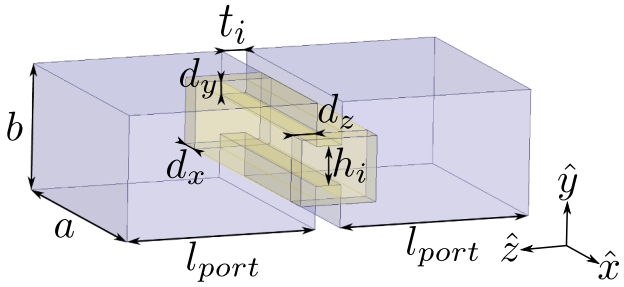

Fig. 3. Proposed impedance inverter and its geometrical parameters. The impedance inverter consists of a classical capacitive iris which is completely filled by a dielectric piece. The base rectangular waveguide, utilized in this paper, is a standard WR-75 ($a = 19.05$ mm and $b = 9.525$ mm). For our designs the dimensions of the dielectric piece are: $d_x = 1$ mm, $d_y = 0.5$ mm and $d_z = 1$ mm, while the iris thickness is $t_i = 1$ mm. It should be noted that the external housing and the dielectric piece are wider than the host waveguide width near the iris (due to assembly reasons), in view of a possible future practical realization (see dimension d_x shown in the figure). The input and output ports are located at a distance l_{port} from the iris.

S-parameters simulations of the structure depicted in Fig. 3, from:

$$|S_{21}| = \frac{2}{\frac{K_i}{Z_0} + \frac{1}{\frac{K_i}{Z_0}}}, \tag{1}$$

being Z_0 the characteristic impedance of the input and output ports, and $|S_{21}|$ the transmission parameter magnitude. Using (1), the values of the impedance inverters are assessed for the structure shown in Fig. 3, as a function of the height of the capacitive iris (h_i). In Fig. 4, five K_i/Z_0 curves are presented considering different types of dielectric materials. It can be observed that the maximum K_i/Z_0 value that can be achieved decreases as the dielectric permittivity of the material increases. This is to be expected, as higher permittivity dielectrics will typically increase the reflection of the electromagnetic waves impinging on the iris. Thus, a dielectric with high permittivity presents limitations if high K_i/Z_0 values are required, which is normally the case for the first and last impedance inverters of a stepped-impedance low-pass filter. Nevertheless, this is not an important problem, since the outermost inverters can be implemented without any dielectric material ($\epsilon_r = 1$ curve in Fig. 4), due to the low multipactor risk associated to the large gaps commonly needed

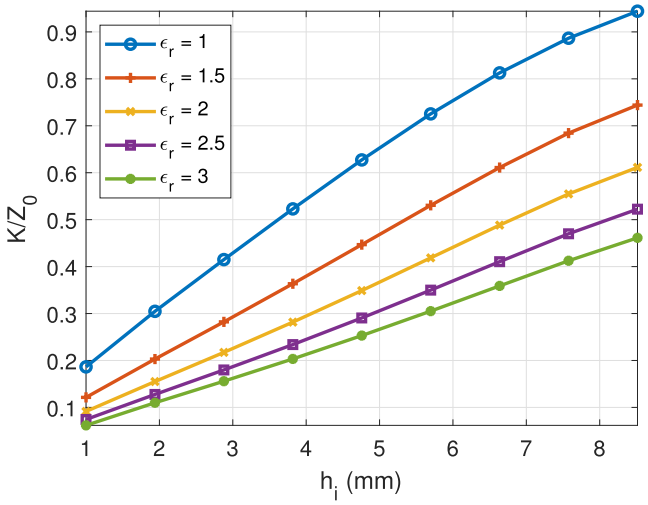

Fig. 4. Normalized impedance inverter (K_i/Z_0) as a function of the height of the capacitive iris (h_i), shown in Fig. 3. Five curves are plotted in order to represent the influence of different materials with relative permittivities ranging from $\epsilon_r = 1$ (which represents a waveguide without any dielectric piece) to $\epsilon_r = 3$. The analysis frequency is $f = 13.25$ GHz.

to model these inverters, as indicated by the lowpass filter synthesis procedure.

The second step of the design procedure is to calculate the distance between the impedance inverters (length of the connecting transmission lines, see Fig. 1). Once the gap h_i has been selected for each impedance inverter of the filter, the phase of the transmission parameter ($\angle S_{21}$) is monitored as a function of the distance from the auxiliar input/output ports to the inverter (l_{port} in Fig. 3). In Fig. 5, the phase curves for the transmission parameter of an impedance inverter, using the same five dielectric pieces as before, are shown. In addition, for reference, we have included in this figure the phase delay introduced by a plain rectangular waveguide with the same overall length $2l_{port} + t_i$. As can be seen, the phase difference between the empty waveguide and those with the inner inverter ranges from 50° to 65°, increasing for higher dielectric permittivities. It is important to highlight that during the design procedure this phase is associated to the rectangular waveguide fundamental mode at the ports. For inverters that are located far from each other with large electrical length θ_c, the main interactions are restricted to this fundamental mode. However, if θ_c is reduced below a certain threshold, the coupling between irises (inverters) originated by reactive modes will be strong enough to degrade the initial lowpass filter response, obtained once the design technique has been applied. This situation requires to apply a final optimization process for achieving the target filter specifications.

These curves are computed for a fixed $K_i/Z_0 = 0.41$. Using this information, the physical distance to the impedance inverter (l_{port}) is adjusted for a phase of the transmission parameter given by:

$$\angle S_{21} = -\theta_c - 90°, \tag{2}$$

where ($-90°$) is the phase shift introduced by an ideal impedance

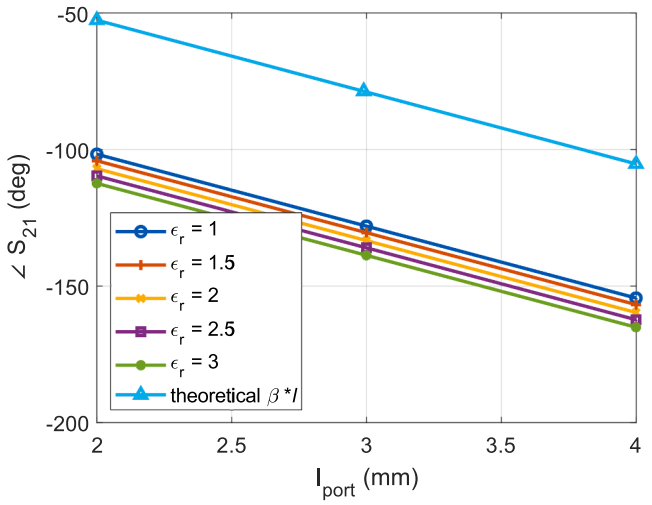

Fig. 5. Transmission parameter phase ($\angle S_{21}$) corresponding to a capacitive iris (t_i length) filled with different permittivity dielectric material pieces placed at l_{port} from the input and output rectangular waveguide ports, as can be seen in Fig. 3. This phase has been compared to that obtained for the fundamental mode of an empty rectangular waveguide with the same total length ($2l_{port} + t_i$). The five curves of the inverters are computed for a dielectric relative permittivity that ranges from $\epsilon_r = 1$ to 3. These curves are calculated maintaining a constant normalized inverter value $K_i/Z_0 = 0.41$. The analysis frequency is $f = 13.25$ GHz.

inverter, and θ_c is the electrical length of the transmission lines connecting the inverters (see Fig. 2).

It should be noted that the inclusion of a dielectric material on the capacitive iris, increases the phase delay with respect to the baseline (filled with air/vacuum) capacitive iris. Therefore, the resultant low-pass filter will be more compact as compared to a similar rectangular waveguide low-pass filter employing only plain (all-metallic) capacitive irises. Furthermore, the utilization of dielectrics with high relative permittivity values is not advisable, since it will lead to inverters very closely spaced. As stated previously, this will lead to stronger interactions and undesired cross coupling effects between the different elements of the filter, and ultimately may render the whole structure impractical, specially if low values of θ_c are chosen.

3. Proposed design example

In this section, we propose a novel rectangular waveguide low-pass filter structure using, as building block, the impedance inverter illustrated in Fig. 3. The sketch of the filter is shown in Fig. 6, and its physical dimensions for two configurations (after the design process and after a final optimization) are given in Table 1. This design is implemented with an order $N = 6$, return losses $RL = 21$ dB, being the electrical distance between the inverters $\theta_c = 35°$. In addition, the cutoff frequency of the filter is fixed at $f_c = 13.5$ GHz. The filter is designed taking as reference a standard rectangular waveguide WR-75 ($a = 19.05$ mm and $b = 9.525$ mm), whereas the dielectric material relative permittivity, utilized in the irises, is $\epsilon_r = 2.2$. This filter has been compared to an all-metallic lowpass design with the same specifications, whose dimensions are included in the last column of Table 1. As can observed, the all-metallic filter is longer than the one made with dielectric material coating the irises. This effect is due to reduced physical length of the impedance inverter sections filled with dielectric as compared to those corresponding to only metallic irises that introduce the same phase shift, as it was shown in Fig. 5.

As can be observed in Fig. 6, the first impedance inverter is not filled by a dielectric material. This is due to the necessity of achieving a large K_i/Z_0 value for the input/output inverters, which cannot be obtained by using high relative dielectric permittivities, as it was previously discussed in Fig. 4. As already mentioned, this does not present a significant inconvience, since the gap in the first inverter is always large, and therefore does not represent an important risk in multipactor breakdown power threshold of the filter. On the other hand, the inner impedance inverters of the filter, exhibiting higher risk of multipactor breakdown, are filled with dielectric material. Thus, the filter is only susceptible to suffer from lateral multipactor that can be produced in the areas located between impedance inverters. However, again, this potential risk is much lower with respect to conventional filter designs, since the electric field intensities in these areas are very low as compared to the electric field intensity close to narrow capacitive gaps.

Fig. 7 displays the scattering parameter magnitudes of the filter

Table 1
Physical Dimensions (mm) of the Waveguide Lowpass Filter Illustrated in Fig. 6 along with its Normalized Impedance Inverter Values. For comparison, the dimensions of an all metallic filter with same specificacions are included in the table.

Filter dimensions	K/Z_0	Initial filter	Optimized filter	All metallic filter
h_1	0.75	5.8	5.3	5.6
h_2	0.53	7.78	7.55	3.48
h_3	0.42	6.19	5.25	2.6
h_4	0.39	5.8	5.15	2.41
l_1		6.78	7.15	6.83
l_2		5.6	5.15	5.89
l_3		5.25	4.6	5.49

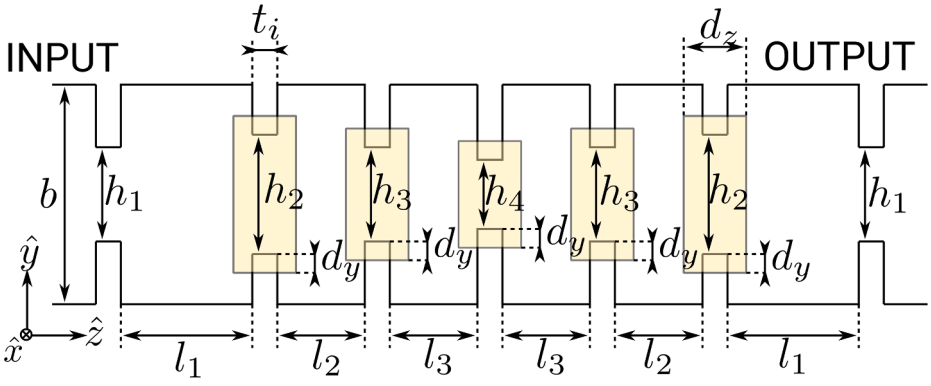

Fig. 6. Sketch, showing the relevant geometrical parameters of a sixth order rectangular waveguide low-pass filter implemented making use of the proposed impedance inverter (see Fig. 3). Table 1 contains the dimensions of the height of the irises and the length of the rectangular waveguide sections, while the rest of the parameters keep the same values as those presented in Fig. 3. For the sake of clarity, the dimension d_x has not been included in this 2D sketch (see Fig. 3).

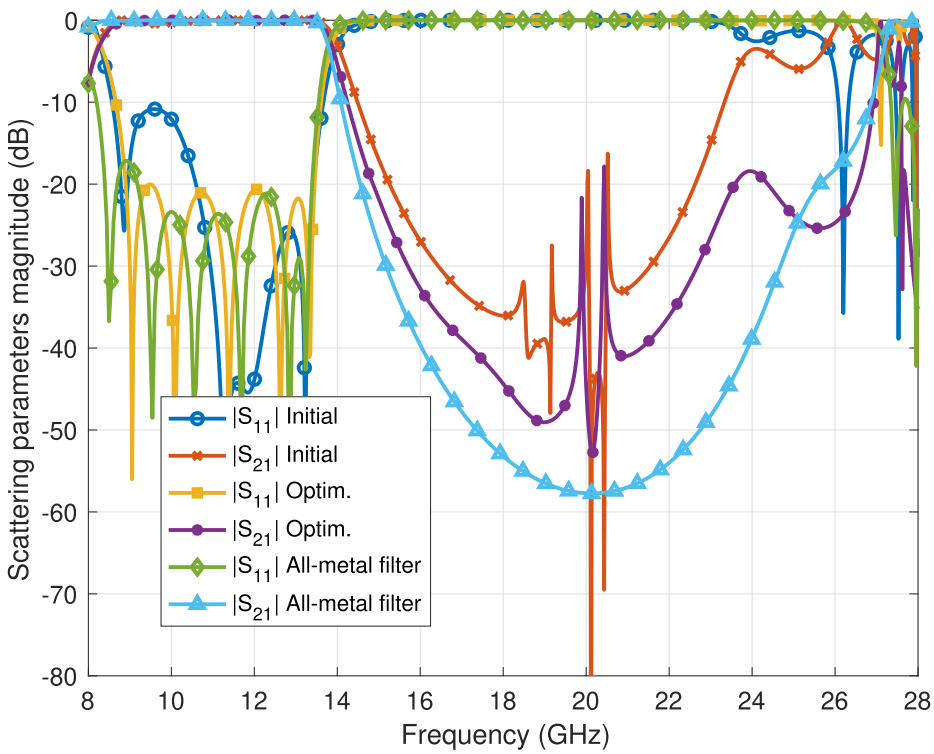

Fig. 7. Scattering parameters magnitudes of the low-pass filter presented in Fig. 6, for two different configurations. The initial configuration is directly obtained after the design process described in Section 2. The final configuration is retrieved after applying a final optimization procedure. This last filter design has been compared to an all-metallic implementation with the same specifications. Losses have not been included in these simulations.

directly obtained after applying the described design procedure, and after performing a final optimization step, clearly showing the effectiveness of the proposed approach. The response, directly obtained after applying the design technique, is not completely equalized. Moreover, some reflection zeros become complex. This is a consequence of the stronger dependence with frequency of the inverters when they are filled by dielectric material. In addition, the distances between the inverters (l_i) are smaller due to the use of dielectric parts, thus causing stronger un-desired cross coupling effects. However, the response is not far from the target specifications. In this respect, a final optimization process can compensate for these effects, as also observed in Fig. 7 (optimized response). The response corresponding to the all metallic filter is also depicted in the figure, matching the same specifications. In this case, the scattering parameters are free of the spurious band appearing from 18 to 21 GHz, and that is associated to spurious resonances due to the interactions of the dielectric material with the capacitive iris.

4. Practical implementation for manufacturing

The presented filter (see Fig. 6) is employed as initial example to design a practical filter for manufacturing (see final design in Fig. 8). This figure shows a sixth order rectangular waveguide low-pass filter along with its relevant geometrical parameters. The resulting dimensions, attained through a final optimization stage, are included in Table 2. The main difference from the first design is the utilization of only one dielectric piece filling all the inner irises of the filter. Despite the fact this is not the best possible solution, it eases the manufacturing process, since it only requires a single dielectric piece. In this regard, the milling process and its final alignment operation with the metallic parts are substantially simplified.

In Fig. 9, two sets of scattering parameters are plotted: one of them is calculated from the filter represented in Fig. 8, whereas the other one corresponds to a traditional rectangular waveguide low-pass filter. The prescribed upper cutoff frequency and bandwidth is the same for the two filters. Although both have been designed with the same upper cutoff

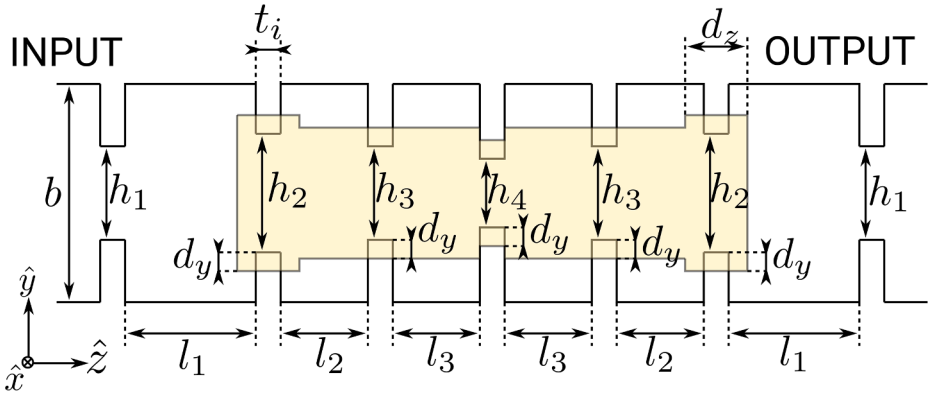

Fig. 8. Sketch, presenting the geometrical parameters of a sixth-order rectangular waveguide low-pass filter implemented by using the proposed impedance inverter (see Fig. 3). Instead of employing five different dielectric pieces, this alternative implementation is made up of only one. Table 2 contains the dimensions of the height of the irises and the length of the rectangular waveguide sections, while the rest of parameters keep the same values as those presented in Fig. 3. For this realization, we have fixed $d_x = 1$ mm (see Fig. 3).

Table 2
Physical Dimensions (mm) of the Rectangular Waveguide Low-pass Filter Illustrated in Fig. 8.

Filter parameters	Dielectric imp. inv. filter	All-metallic filter
h_1	4.7	5.72
h_2	5.4	3.69
h_3	3.1	2.8
h_4	2.9	2.58
l_1	5.85	7.42
l_2	3.31	6.48
l_3	2.26	6.05

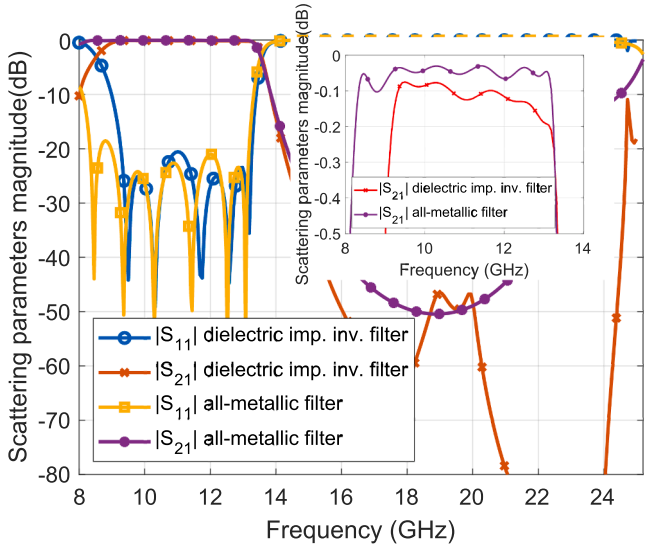

Fig. 9. Simulated scattering parameters magnitude corresponding to the low-pass filter filled with dielectric used as baseline for the manufacturing process, depicted in Fig. 8, alongside those computed for an all-metallic lowpass filter design of the same order, bandwidth and out of band response. In these simulations, the effect introduced by the real lossy dielectric (Teflon) and metallic (Aluminum) materials have been taking into account in order to evaluate the insertion losses in each case (see inset figure).

frequency, there exists some slight differences in the lower frequency region within the passband, due to the dispersive behavior of rectangular waveguides close to their cutoff frequency. For these simulations, we have taken into account the attenuation introduced by the lossy materials used in the manufactured filter prototype (see Fig. 11) (Aluminum and Teflon). As can be observed in the inset of Fig. 9 the insertion losses within the passband corresponding to the lowpass filter with dielectric pieces are slightly higher (0.1 dB in the worst case) than those estimated for the all-metallic filter. On the other hand, a spurious frequency band below -40 dB appears within the stop band of the filter made with dielectric material coating the irises, from 17 to 21 GHz (see Fig. 9). We have investigated the source of this spurious band and found that it is associated to field resonances due to the interaction of the dielectric material with the capacitive irises. Fortunately, the negative effect of these resonances is greatly reduced in real lossy materials.

The low-pass filter, making use of plain (all-metallic) capacitive irises as impedance inverters, is designed to match the same passband specifications and spurious free-range, as the first filter. Its physical dimensions are collected in Table 2 (third column). It should be noted that the lengths (l_i) required for this filter are larger than those needed in the dielectric filled filter. In fact, the filter with dielectric parts compared to the one implemented with plain capacitive irises offers a 36% footprint reduction.

It is also interesting to note that the dielectric filled irises require larger gaps between metallic parts (h_i), than those needed in plain irises. This is due to the extra reflection caused by the dielectric pieces, as discussed in Fig. 4. This is an important advantage of the proposed idea, since it can lead to geometries that avoid too narrow gaps, and therefore are simpler to fabricate. In particular, the smallest gap height in the baseline filter (all-metallic) is $h_4 = 2.58$ mm. However, this value increases to $h_4 = 2.9$ mm if an equivelent dielectric filled filter design is implemented.

A multipactor simulation for the baseline (all metallic) filter, as a function of frequency within the passband, was performed by using the commercial electromagnetic full-wave software CST-FEST3D 2021 Dassault-Systemes [25] high-power module (see Fig. 10) obtaining an estimated 4 kW multipactor breakdown power threshold at $f = 13$ GHz, selected for our experimental multipactor test. As can be observed in this figure, the lowest estimated multipactor breakdown power threshold is close to the rectangular waveguide and filter cutoff frequencies (9 GHz and 13 GHz, respectively). This is the typical behavior in most microwave filters. These results were obtained considering that the filter is made of aluminum in terms of SEY. As expected, the simulation software showed that the lowest multipactor breakdown power threshold occurs in the central impedance inverter, with the smallest air gap.

The designed filter is finally realized with Teflon, since this dielectric material admits a simple mechanization process using standard milling techniques. The metallic parts of the filter were built using aluminum. Photographs of the manufactured hardware are shown in Fig. 11. In Fig. 12, the results retrieved from simulations are illustrated, comparing them with those measured in the real manufactured hardware. One should keep in mind that this last lowpass filter implementation, based on the structure presented in Fig. 8, differs from the one employed during the design stage (see Fig. 6) in how the dielectric material is used to fill the irises. Whereas in Fig. 6, there exist separate dielectric pieces located at the different irises, in Fig. 8, to simplify the manufacturing process, a single dielectric part filling simultaneously several irises has been employed. In this second case, the filter is first designed with separate dielectric pieces, and then all pieces are joined together in a single piece. In this last operation a final optimization procedure is needed to correct the initial design. Although the design process is more complicated, subsequent manufacturing and assembling operations are substantially simplified.

Both filter responses (simulated and measured) show good agreement. With respect to the target response illustrated in Fig. 9, the manufactured filter exhibits slightly larger bandwidth with a cut-off

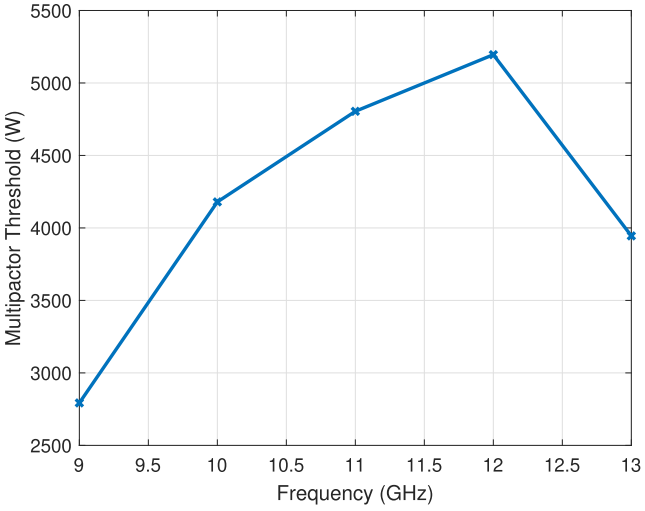

Fig. 10. Multipactor Breakdown Power Threshold as a function of frequency within the filter passband computed by the commercial software CST-FEST3D high-power module. The experimental multipactor test was carried out at $f = 13$ GHz.

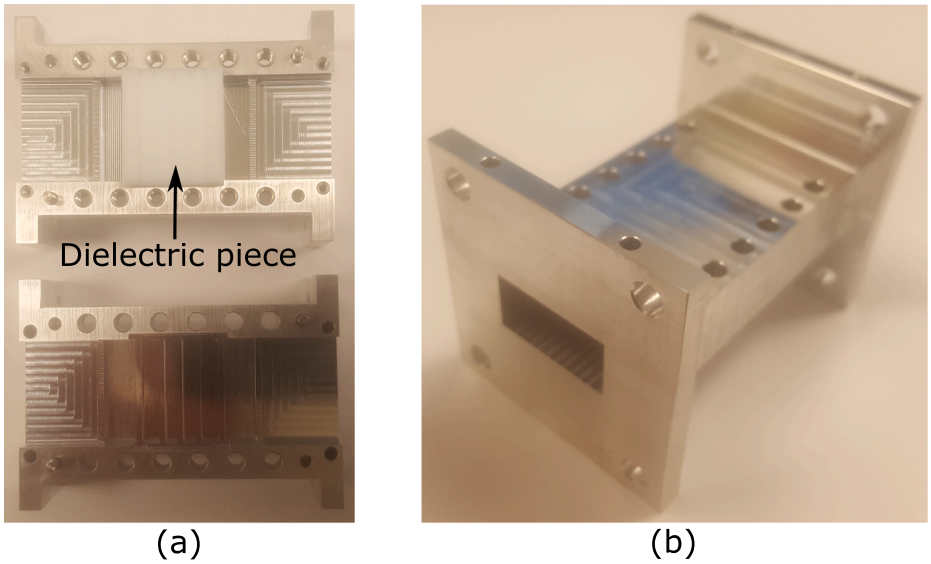

Fig. 11. Photographs of the manufactured prototype. (a) Filter before the assembly, presenting details of the aluminum housing. The picture shows how the dielectric piece is easily aligned in the filter housing. (b) View of the assembled filter.

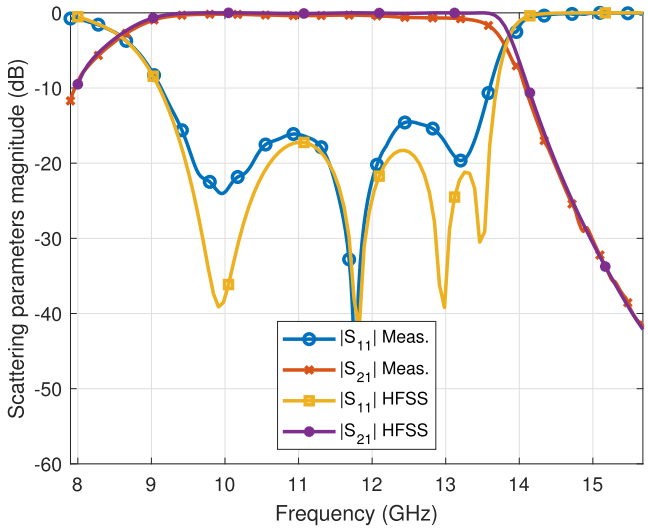

Fig. 12. Scattering parameters magnitudes of the lowpass filter presented in Fig. 8, implemented with Teflon. The measured results, corresponding to the manufactured filter, show good agreement with those calculated by the electromagnetic simulation software HFSS (Ansys [28]).

frequency of 13.6 GHz.

Also, the return loss level ($RL = 15$ dB) is lower than expected. The insertion losses are $IL = 0.32$ dB. These small deviations, between the HFSS simulation of the filter and the measured prototype, are due to a slight difference in the permittivity of the Teflon ($\epsilon_r = 2.1$ instead of $\epsilon_r = 2.2$), and to errors in the milling process and during the assembling/alignment operations of the dielectric piece. In spite of these problems, the performance of the manufactured filter is quite acceptable.

Furthermore, we have performed a detailed study on how the different parts of the filter contribute to the total losses. For the filter which was manufactured, we found that approximately 68% of the total losses are due to the dielectric piece, and the other 32% are due to metallic parts (waveguide walls and capacitive irises). In addition, we found that losses can be lowered if less dielectric pieces are employed, filling only the most critical gaps in the structure. However, multipactor effects can be triggered in the gaps without dielectric pieces, thus lowering the overall multipactor power threshold in the structure. Therefore, there is a clear trade-off between these two factors.

Although poorer filter return losses could be translated into a higher measured multipactor breakdown power threshold due to the mismatch between the test power generator and DUT, the difference would not be significant with respect to the filter designed and simulated with prescribed return losses higher than 20 dB (see Fig. 9). In our case the lower measured return losses are around 15 dB, resulting in a measured multipactor breakdown power threshold that would only be a 2% higher than that corresponding to the filter with $RL > 20$ dB.

The manufactured filter was tested at ESA-VSC [26] multipactor testbed. The measurements confirmed that the multipactor breakdown effect is not triggered up to the maximum power admitted by the experimental facility (5.5 kW) at $f = 13$ GHz. On the contrary, as already discussed, the reference filter made up of plain metallic inverters shows a 4 kW breakdown threshold at the same frequency. Even though our experiments could only test a maximum input power of 5.5 kW, a close to an order of magnitude higher threshold is expected, due to the blockage effect of electrons in critical gap areas, as was demostrated in Hu and Cui [23] for a dielectric filled E-plane impedance transformer.

A similar strategy could be followed in order to improve the multipactor breakdown power threshold of bandpass inline capacitive filters. In this case, the design process leads to very narrow gaps that are prone to trigger multipactor at low powers. However, these gaps could also be coated by dielectric material, following a similar strategy. We have found that in this case, the multipactor breakdown power level would be similar to an inductive bandpass filter with the same specifications. We have conducted a preliminary study on this type of bandpass filters, and have observed that the capacitive design is bulkier and lossier than its inductive counterpart. Therefore bandpass filters with capacitive irises may not be the best choice for space communication applications. On the other hand, the preliminary study has shown that the capacitive bandpass filter alternative leads to a higher selectivity as compared to the inductive solution.

5. Conclusion

In this work, a novel rectangular waveguide low-pass filter with a high multipactor breakdown power threshold has been presented and experimentally validated. It is proved that the use of dielectric materials to implement low-pass filters results in capacitive irises with larger gaps between metallic pieces. Moreover, the dielectric pieces avoid free

electrons movement in those critical areas. Thus, the multipactor breakdown effect will not be triggered in the small gaps of the structure, where the electromagnetic fields are usually very intense. Furthermore, the distance between the capacitive irises is noticeably reduced, thus this kind of filters has more compact sizes than those obtained with plain (all-metallic) capacitive irises. A filter prototype was manufactured and measured, showing no multipactor breakdown up to the maximum power that could be tested by the experimental testbed (5.5 kW). This is a significant improvement as compared to an equivalent rectangular waveguide filter based on plain capacitive irises, which was limited to 4 kW. We believe that this kind of filters could be extremely useful for high-power satellite communication systems, where the multipactor breakdown risk could be a critical aspect.

Declaration of Competing Interest

The authors declare that they have no known competing financial interests or personal relationships that could have appeared to influence the work reported in this paper.

Acknowledgment

This research work has been financially supported by the Spanish *Ministerio de Ciencia e Innovación* in the frame of the project "*Green an Efficient Technologies for Advanced Telecommunication Systems (GRETAS)*" with Ref. TPID2019-103982RB-C42.

References

[1] Cameron RJ, Kudsia CM, Mansour RR. Microwave Filters for Communication Systems: Fundamentals Design and Applications. 2nd ed. Wiley; 2018. ISBN: 9781118274347.
[2] Vaughan J. Multipactor. IEEE Trans Electron Devices 1988;35:1172–80. https://doi.org/10.1109/16.3387.
[3] Gallagher WJ. The multipactor effect. IEEE Trans Nucl Sci 1979;26:4280–2. https://doi.org/10.1109/tns.1979.4330768.
[4] San-Blas A, Gimeno B, Boria V. Study of the multipactor phenomenon using a full-wave integral equation technique. AEU - Int J Electron Commun 2017;79:286–90. https://doi.org/10.1016/j.aeue.2017.06.009.
[5] Pinheiro-Ortega T, Monge J, Marini S, Sanz J, Sorolla E, Mattes M, et al. Microwave corona breakdown prediction in arbitrarily-shaped waveguide based filters. IEEE Microwave Wirel Compon Lett 2010;20:214–6. https://doi.org/10.1109/lmwc.2010.2042555.
[6] Gharehkand FK. Design of a 16 way radial microwave power divider/combiner with rectangular waveguide output and coaxial inputs. AEU - Int J Electron Commun 2014;68:422–8. https://doi.org/10.1016/j.aeue.2013.11.005.
[7] Walker C, El-Gomati M, Assad A, Zadrazil M. The secondary electron emission yield for 24 solid elements excited by primary electrons in the range 250–5000 eV: a theory/experiment comparison. Scanning 2008;30:365–80. https://doi.org/10.1002/sca.20124.
[8] Wolk D, Vicente C, Hartnagel HL, Mattes M, Mosig JR, Raboso D. An investigation of the effect of fringing fields on multipactor breakdown. In: 5th International Workshop on Multipactor, Corona and Passive Intermodulation in Space RF Hardware, 2005, p. 93–99.
[9] Al-Mudhafar A, Puech J, Hartnagel H. Investigation of multipactor effect in microwave components in the presence of fringing fields. In: 2014 44th European Microwave Conference, IEEE, 2014. doi:10.1109/eumc.2014.6986456.
[10] Udiljak R, Anderson D, Lisak M, Puech J, Semenov VE. Multipactor in a waveguide iris. IEEE Trans Plasma Sci 2007;35:388–95. https://doi.org/10.1109/tps.2007.892737.
[11] Gonzalez-Iglesias D, Soto P, Anza S, Gimeno B, Boria V, Vicente C, Gil J. Multipactor susceptibility charts for ridge and multiridge waveguides. IEEE Trans Electron Devices 2012;59:3601–7. https://doi.org/10.1109/ted.2012.2215611.
[12] Vera-Castejon P, Correas-Serrano D, Quesada-Pereira FD, Hinojosa J, Alvarez-Melcon A. A novel low-pass filter based on rounded posts designed by an alternative full-wave analysis technique. IEEE Trans Microw Theory Tech 2014;62:2300–7. https://doi.org/10.1109/tmtt.2014.2341661.
[13] Gonzalez JH, Garcia-Baquero DR, Ernst C, Schmitt D, Esbert VB, Martinez BG, et al. Optimized multipactor-resistant wedge-shaped waveguide bandpass filters. IEEE Trans Plasma Sci 2013;41:2135–44. https://doi.org/10.1109/tps.2013.2253134.
[14] Hueso J, Raboso D, Schmitt D, Boria VE, Martinez B, Vicente C. Study of the multipactor effect in bandpass wedge-shaped waveguide filters. IEEE Trans Electron Devices 2011;58:3205–12. https://doi.org/10.1109/ted.2011.2159610.
[15] Hueso J, Vicente C, Gimeno B, Boria V, Marini S, Taroncher M. Multipactor effect analysis and design rules for wedge-shaped hollow waveguides. IEEE Trans Electron Devices 2010;57:3508–17. https://doi.org/10.1109/ted.2010.2075931.
[16] Arregui I, Anza S, Arnedo I, Vicente C, Lujambio A, Gil J, et al. Multipactor prediction in novel high-power low-pass filters with wide rejection band. In: 2009 European Microwave Conference (EuMC), 2009, p. 675–78. doi:10.23919/EUMC.2009.5296447.
[17] Arregui I, Arnedo I, Lujambio A, Chudzik M, Benito D, Jost R, et al. A compact design of high-power spurious-free low-pass waveguide filter. IEEE Microwave Wirel Compon Lett 2010;20:595–7. https://doi.org/10.1109/lmwc.2010.2072989.
[18] Arregui I, Teberio F, Arnedo I, Lujambio A, Chudzik M, Benito D, et al. High-power low-pass harmonic filters with higher-order TE_{n0} and non-TE_{n0} mode suppression: Design method and multipactor characterization. IEEE Trans Microw Theory Tech 2013;61:4376–86. https://doi.org/10.1109/tmtt.2013.2288208.
[19] Gonzalez-Iglesias D, Gimeno B, Boria VE, Gomez A, Vegas A. Multipactor effect in a parallel-plate waveguide partially filled with magnetized ferrite. IEEE Trans Electron Devices 2014;61:2552–7. https://doi.org/10.1109/ted.2014.2322395.
[20] Coves A, Torregrosa-Penalva G, Vicente C, Gimeno B, Boria V. Multipactor discharges in parallel-plate dielectric-loaded waveguides including space-charge effects. IEEE Trans Electron Devices 2008;55:2505–11. https://doi.org/10.1109/ted.2008.927945.
[21] Gonzalez-Iglesias D, Gomez A, Gimeno B, Fernandez O, Vegas A, Casas F, et al. Analysis of multipactor RF breakdown in a waveguide containing a transversely magnetized ferrite. IEEE Trans Electron Devices 2016;63:4939–47. https://doi.org/10.1109/ted.2016.2614370.
[22] Torregrosa-Penalva G, Coves Á, Martinez BG, Montero I, Vicente C, Boria VE. Multipactor susceptibility charts of a parallel-plate dielectric-loaded waveguide. IEEE Trans Electron Devices 2010;57:1160–6. https://doi.org/10.1109/ted.2010.2043182.
[23] Hu T, Cui W. Design and multipactor analysis of microwave impedance transformer with dielectric filling. In: The 8th European Conference on Antennas and Propagation (EuCAP 2014), IEEE, 2014. doi:10.1109/eucap.2014.6902056.
[24] Vague J, Melgarejo JC, Guglielmi M, Boria VE, Anza S, Vicente C, et al. Multipactor effect characterization of dielectric materials for space applications. IEEE Trans Microw Theory Tech 2018;66:3644–55. https://doi.org/10.1109/tmtt.2018.2845869.
[25] Dassault-Systemes, CST Studio Suite, FEST3D 2021, https://www.3ds.com/products-services/simulia/products/fest3d/, 2021.
[26] ESA-VSC, High Power RF Space Laboratory, https://www.val-space.com/en/esa-vsc-european-high-power-radiofrequency-space-laboratory, 2021.
[27] Mximo-Gutirrez C, Hinojosa J, Alvarez-Melcon A. Design of wide band-pass substrate integrated waveguide (siw) filters based on stepped impedances. AEU - Int J Electron Commun 2019;100:1–8. https://doi.org/10.1016/j.aeue.2018.12.022.
[28] Ansys, Ansys HFSS, https://www.ansys.com/products/electronics/ansys-hfss, 2021.